Porous aerosol in degassing plumes of Mt. Etna and Mt. Stromboli

Valery Shcherbakov[1,2], Olivier Jourdan[1], Christiane Voigt[3,4], Jean-Francois Gayet[1], Aurélien Chauvigne[1], Alfons Schwarzenboeck[1], Andreas Minikin[3,*], Marcus Klingebiel[4,5], Ralf Weigel[4], Stephan Borrmann[4], Tina Jurkat[3], Stefan Kaufmann[3], Romy Schlage[3], Christophe Gourbeyre[1], Guy Febvre[1], Tatyana Lapyonok[6], Wiebke Frey[7,**], Sergej Molleker[7], Bernadett Weinzierl[3,8]

[1]Laboratoire de Météorologie Physique, UMR 6016 CNRS/Université Clermont Auvergne, Clermont-Ferrand, France.
[2]LaMP, Institut Universitaire de Technologie d'Allier, Montluçon, France.
[3]Institut für Physik der Atmosphäre, Deutsches Zentrum für Luft- und Raumfahrt (DLR), Oberpfaffenhofen, Germany.
[4]Institut für Physik der Atmosphäre, Johannes Gutenberg-Universität Mainz, Mainz, Germany.
[5]Max Planck Institute for Meteorology, Hamburg, Germany.
[6]Laboratoire d'Optique Atmosphérique, UMR 8518 CNRS/Université des Sciences et Technologies de Lille, Villeneuve d'Ascq, France.
[7]Max Planck Institute for Chemistry, Particle Chemistry Department, Mainz, Germany.
[8]University of Vienna, Faculty of Physics, Aerosol Physics and Environmental Physics, Vienna, Austria.
[*]Now at Flugexperimente, Deutsches Zentrum für Luft- und Raumfahrt (DLR), Oberpfaffenhofen, Germany.
[**]Now at The University of Manchester, Centre for Atmospheric Science, Manchester, UK.

Correspondence to: Valery Shcherbakov (v.shcherbakov@opgc.univ-bpclermont.fr)

Abstract. Aerosols of the volcanic degassing plumes from Mt. Etna and Mt. Stromboli were probed with *in situ* instruments on board the Deutsches Zentrum für Luft- und Raumfahrt research aircraft Falcon during the contrail, volcano, and cirrus experiment CONCERT in September 2011. Aerosol properties were analyzed using angular scattering intensities and particle size distributions simultaneously measured with the Polar Nephelometer and the Forward Scattering Spectrometer probes (FSSP series 100 and 300), respectively. Aerosols of degassing plumes are characterized by low values of the asymmetry parameter (between 0.6 and 0.75); the effective diameter was within the range of 1.5 – 2.8 µm and the maximal diameter was lower than 20 µm. A principal component analysis applied to the Polar Nephelometer data indicates that scattering features of volcanic aerosols of different crater origins are clearly distinctive from angular scattering intensities of cirrus and contrails. Retrievals of aerosol properties revealed that the particles were "optically spherical" and the estimated values of the real part of the refractive index are within the interval from 1.35 to 1.38. The interpretation of these results leads to the conclusion that the degassing-plumes aerosols were porous with air voids. Our estimates suggest that aerosol particles contained about 18 to 35 % of air voids in terms of the total volume.

1 Introduction

The impacts of continuously degassing volcanoes on the environment and human health are well recognized (Delmelle, 2003; Mather et al., 2004). Fumarolic plumes of passively degassing volcanos are strongly involved in the deposition and redistribution of metals and trace elements (Fulignati et al., 2006). Degassing volcanoes have a potentially large effect on the natural background aerosol loading and the radiation budget of the atmosphere (Schmidt et al., 2012; Oppenheimer et al., 2011).

The size-resolved chemical composition, morphology and particle size distribution of volcanic aerosols are important in defining their effects on the atmosphere, environment and human health. A description of the various techniques used in the characterization of 'near-source' volcanic particles as well as a review of field-campaigns results are given by Mather et al., (2004). The morphology of atmospheric and volcanic-plumes aerosols was studied mostly by electron microscopy and x-rays spectroscopy (see, e.g., Pósfai et al., 1999; Obenholzner et al., 2003; Mather et al., 2004; Martin et al., 2008). Due to the high spatial resolution of such instruments, it was evidenced that complex composition, irregular shape, intricate internal structure, and random surface roughness are the rule rather than the exception for aerosol particles. At the same time, the quasi-spherical particles are not uncommon (see, e.g., Obenholzner et al., 2003).

The overwhelming majority of works dealing with internal structure of aerosol particles consider a mixture of chemical compounds (see, e.g., Nousiainen, 2009; Ulanowski and Schnaiter, 2011; and references therein). To date, literature on porous aerosol is rather limited. Jeong and Nousiainen (2014) demonstrated, using transmission electron microscopy analysis, that the internal structures of individual Asian dust particles were formed by the patterned arrangement of nano-to-micron-sized mineral grains and pores. Highly-porous aerosol particles, obtained from proxies for organic compounds, were investigated by Adler et al. (2013, 2014) with focused ion beam - scanning electron microscopy techniques and a cavity ring down system. Most of the information on volcanic vesicular, i.e., porous ash particles was obtained from samples collected at the ground level. A compilation of the morphological features of volcanic ash particles derived through the use of scanning electron microscopy was done by Heiken and Wohletz (1985).

Generally, scattering matrices of irregular or/and heterogeneous particles have to be modelled on the base of the exact electromagnetic wave theory (see, e.g., Mishchenko et al., 2000). On the other hand, heterogeneous materials could be treated similar to homogeneous substances when the typical dimension d of their inhomogeneity is much smaller than the wavelength λ of the considered radiation, $d<<\lambda$ (Chýlek et al., 2000), that is, using effective medium approximations (EMAs). The applicability of EMAs for calculating scattering properties of inhomogeneous atmospheric particles was verified in the recent work by Liu et al. (2014) by comparing with the standards-of-truth provided by calculations based on the pseudo-spectral time domain method (PSTD). The exact heterogeneous mixing structures of non-absorptive or weakly absorptive particles were considered in the PSTD calculations. Liu et al. (2014) concluded that scattering properties of the equivalent homogeneous particles agree well with those of internally mixed particles. Fundamental aspects and recent developments of the scattering of electromagnetic radiation by a discrete random medium as well as applicability of the EMAs are reported in the work by Mishchenko et al., 2016.

Of course, it is hardly probable that EMAs are able to provide all elements of a scattering matrix with high accuracy for any value of the scattering angle θ. But, it is feasible to perform modeling with

admissible errors, especially when one deals with angular scattering intensities within a limited interval of θ. For example, the works by Chylek et al. (1988) and Kolokolova and Gustafson (2001) showed acceptable agreement between experimental results and EMA calculations.

Remote sensing methods, namely, sun photometry, lidar sounding and satellite observations are largely employed for volcanic-plumes studies. Generally, such techniques are related to inverse problems, i.e., retrievals of aerosols characteristics on the base of measured optical signals. Consequently, values of the aerosol refractive index have to be estimated with a retrieval code or specified a priori, i.e., preassigned. When values are preassigned, the refractive index of bulk matter or sulfuric acid solutions are commonly used (see, e.g., Watson and Oppenheimer, 2000, 2001; Spinetti et al., 2007; Kahn et al., 2007; Martin et al., 2009; Marenco et al., 2011; Young et al., 2012). Examples, where the refractive index was retrieved along with a size distribution, can be found in the works by Toledano et al. (2012); Waquet et al., (2014), and references therein. Effective medium approximations were used in inverse problems by Abo Riziq et al. (2007) and Adler et al. (2013, 2014) where refractive indices of laboratory-generated aerosols were retrieved by comparing the measured size-resolved extinction-efficiency with Mie-theory calculations.

This work is devoted to aerosol optical characteristics of the volcanoes Mt. Etna and Mt. Stromboli degassing plumes, retrievals of size distributions and refractive-index values, and consequent inferences about morphological properties of aerosols. In the following, the aircraft instrumentation and the measurements conditions are outlined first. Section 3 addresses the outcomes of the Principal Component Analysis in details. Section 4 describes a careful approach to derive size-distributions and refractive-index as well as the results. Section 5 is devoted to discussion and inferences.

2 Instrumentation and flight overview

This study addresses *in situ* measurements in degassing plumes from the volcanoes Mt. Etna and Mt. Stromboli performed during the CONCERT (contrail, volcano and cirrus experiment) campaign in 2011 (Voigt et al., 2014a). Particles and trace gases of the volcanic plumes were probed with instruments on board the DLR (Deutsches Zentrum für Luft- und Raumfahrt) research aircraft Falcon. Descriptions of the instrumentation of the two CONCERT campaigns in 2008 and 2011 are given in Voigt et al. (2010, 2011, 2014a); individual instruments are discussed in detail by Frey et al., (2011); Gayet et al., (2012); Jeßberger et al., (2013); Kaufmann et al., (2014); Kaufmann et al., (2016) and Jurkat et al., (2016). In addition to the instrumentation of the CONCERT campaign in 2008 (Voigt et al., 2010), the FSSP-100 forward scattering spectrometer probe was employed during the CONCERT campaign in 2011. Below, we briefly describe the instruments used for our study.

2.1 Particle probes

The Polar Nephelometer (PN) (Gayet et al., 1997) measures the angular scattering intensities (ASIs) of an ensemble of particles ranging from less than 1 micrometer to about 1 mm diameter, which intersect a collimated laser beam (λ = 804 nm) near the focal point of a parabolic mirror. Observations are usually limited to 32 scattering angles θ near-uniformly positioned from 15° to 162°. Measurements at nearly forward and backward directions (θ < 15° and θ > 162°) are not reliable due to the diffracted light pollution caused by the edges of holes drilled on the paraboloidal mirror (see, e.g, Jourdan et al., 2010). The sampling volume is defined by the cross sectional area of the beam (10 mm long and 5 mm diameter) multiplied by a linear speed of air populated with particles passing through the instrument. Direct measurement of the ASIs allows particle types (droplets or non-spherical particles) to be distinguished and calculation of the optical parameters to be performed (extinction coefficient *Ext* and asymmetry parameter *g*, see Gayet et al., 2002). Generally, the *g*-value decreases with increasing non-sphericity of the particles all other parameter being the same (Gayet et al., 2002; Gayet et al., 2012). The accuracies of the extinction coefficient and asymmetry parameter are 25% and 4% respectively (Jourdan et al., 2010; Gayet et al., 2012).

The FSSP-300 and FSSP-100 forward scattering spectrometer probes (Baumgardner et al., 1992; Petzold et al., 1997; Frey et al., 2011) measure the intensity of light scattered by single particles in forward direction at angles from 6° to 15° (Jeßberger et al., 2013), which is governed mainly by diffraction and therefore depends on (i) the refractive index of the particles, and (ii) the projected area of the particle which itself depends on the particle shape. Indeed, the size calibration for non-spherical particles is expressed in terms of equivalent surface diameter, i.e. the diameter of a sphere that has the same projected area (Mishchenko et al., 1997). The FSSP-300 signal is resolved into an array of 31 channels in the size range of 0.35 to 38.6 µm. The signal is then converted into a corresponding particle size using water droplet response (the refractive index of 1.33). Because of the ambiguities in the Mie scattering curve, the FSSP-100 size-distributions have been rebinned to 14 size bins in the diameter range from 1.02 to 47.05 µm (water droplet).

2.2 Trace-gas instruments

The trace gases SO_2, HCl, and HNO_3 were measured by the Airborne chemical Ionization Mass Spectrometer AIMS (Voigt et al., 2014a; Jurkat et al., 2016) equipped with an inlet system and a custom made ion source generating SF_5^- reagent ions (Jurkat et al., 2010). Air is drawn into the backward-facing perfluoroalkoxy (PFA) inlet using a pumping system. In the high-voltage gas discharge ion source SF_5^- ions are produced from a flow of SCF_8 in N_2 at pressures controlled to 40 hPa. The SF_5^- ions react selectively with trace species to form product ions via a fluoride transfer reaction (Jurkat et al., 2011). The ions pass three differentially pumped vacuum chambers of the mass spectrometer system, before they are detected with a channeltron detector. An in-flight calibration is performed by adding a

permanent flux of isotopically labeled $^{34}SO_2$ to the inlet line. Further, HNO_3 and HCl were calibrated in the laboratory after the flights. Accuracies of 17–36% were achieved for SO_2, 33–35% for HCl, and 18–36% for HNO_3, mainly depending on dilution of the inlet flow (Voigt et al., 2014a; Voigt et al., 2014b).

Water vapor was measured with the tunable diode laser system WARAN (WAter vapoR ANalyzer), which primarily consists of a commercial WVSS-II water vapor sensor (SpectraSensors Inc.) (Kaufmann et al., 2014) with the measurement range from 30 to 40000 ppmv. In the measurement cell, a laser is tuned over the water vapor absorption line at 1.37 µm and the water vapor mixing ratio is determined from the absorption signal. The passive sample flow through the system is realized using a Rosemount inlet. The water vapor mixing ratio is measured with a relative uncertainty < 6 % at 2.4 s time resolution and for water vapor mixing ratios above 500 ppmv relevant for the low-altitude flight legs shown here. The instrument is calibrated before and after the campaign using a frost point hygrometer (MBW373LX) as the reference. The uncertainty of 0.5°K in the static air temperature measurement translates to a relative uncertainty of around 4% in the saturation pressure over water. Adding both contributions, the relative humidity with respect to water (RH_w) can be determined with a relative uncertainty of a RH_w value generally less than 10 %.

2.3 Flight overview

Degassing plumes from the volcanoes Mt. Stromboli and Mt. Etna were probed on 30 September 2011 (from 6:50 to 8:40 UTC). Visual observations from the cockpit of the Falcon showed that there was one single plume degassing from the Mt. Stromboli; whereas there were two distinct degassing plumes from the Mt. Etna, see Fig. 1(a). The Etna plumes were spreading at two different altitudes and they originated from at least two craters, namely, North East crater (upper plume) and Bocca Nuova crater (lower plume) (Voigt et al., 2014a). From the four main craters at Mt. Etna, these two craters were identified as the major emitters on that day. The Falcon flight track over Sicily is shown in Fig. 1(b). It was set up to probe the two Etna plumes and the Stromboli plume.

Figure 2 shows time series of trace-gases measurements, flight altitude, extinction coefficient and asymmetry parameter both derived from the Polar Nephelometer measurements. The very low relative humidity has to be particularly emphasized. The values of RH_w are lower than the crystallization humidity of most sulfates, nitrates and chlorides (see, e.g., Tang and Munkelwitz, 1991). In other words, the plumes were spreading in the dry troposphere. In addition, the air temperatures within the plumes were always above the freezing point, i.e., > 273.15°K. The extinction-coefficient series reveals several peaks that correspond to the time intervals when the research aircraft was probing the degassing plumes (see shaded areas in Fig. 2). The close correspondence between the extinction coefficient and the time series of the trace gases HNO_3, SO_2, HCl is evident in Fig. 2. The trace-gas composition of the volcanic plumes has been investigated by Voigt et al., (2014a). Different trace gas mixing ratios of CO_2/SO_2 and SO_2/HCl has been identified in the volcanic plumes from North East and Bocca Nuova craters.

Specifically, it is shown that neither SO_2 conversion to sulfate nor HCl uptake in sulfate aerosol play a major role in the aging plume under dry tropospheric conditions.

3 PCA analysis of Polar-Nephelometer data

In this section, a statistical tool, the Principal Component Analysis (PCA) is applied to the Polar Nephelometer data obtained during the CONCERT campaign in 2011. It should be emphasized that the peculiarity of the PN data recorded within the quiescent degassing volcanic plumes is that the signals were quite low, at least much lower than those ones registered within contrails and clouds. We recall that during particle samplings, the Polar Nephelometer raw signals are superimposed on the background signals (or zero baselines), which are due to electronic or optical noises. As a consequence, the accurate subtraction of the background signals was of utmost importance (see Shcherbakov et al., 2006). Thus, the corresponding data were preprocessed with special-purpose software and operator supervision of the data-treatment quality, i.e., wavelet denoising technique.

3.1 Clustering techniques

We employed the PCA to carry out the cluster analysis (see, e.g., Jolliffe, 2002, Ch. 9; Jourdan et al. 2010), that is, to separate the recorded angular scattering intensities (ASIs) into clusters. The advantage of the PCA consists in the fact that it is self-sufficient; in other words, no a priori hypotheses are needed, the clustering is only based on internal properties of a data set. In brief, the PCA is an unsupervised method used to explore the intrinsic variability of the data.

The PCA is particularly fruitful when one deals with high-dimensional data. The PCA provides the possibility to capture much of the total data variation in a few dimensions and to organize observed data into meaningful clusters. That is, with PCA technique, each vector of the data can be represented adequately by a few coefficients, usually three, which correspond to eigenvectors of a covariation matrix. This is especially true when a limited number of primary physical parameters have a major impact on the measured functions (in our case, angular scattering intensities). The obtained coefficients can be used in visualization of the data by scatter plots.

Algebraically, principal components could be defined as particular linear combinations of a set of variables. These linear combinations represent the selection of a new coordinate system obtained by rotating the original system of coordinates. The new axes correspond to the directions with maximum variability and provide a simpler description of the covariance structure of the original set of variables (Johnson and Wichern, 1998).

The peculiarity of our approach is that the log-transformation is applied to the angular scattering intensities before the PCA is carried out (see details in Jourdan et al., 2003; Shcherbakov et al., 2005). The reason for such a preprocessing is the following. In contrast to phase functions, ASIs are not normalized, e.g., they are proportional to the particle concentration. In addition, the ASIs values, as well

as the variances, at the forward angles, as a rule, are of orders of magnitude higher than that ones at the sideward and backward angles. In such conditions, the conventional PCA yields the first principal components that only follow the variance at the forward angles; they do not reproduce all the ASIs variability. The preprocessing, that is, the logarithm of ASIs values makes the variances to be comparable at all angles. In the strict sense, the log-transformation leads to the multiplicative model of the variance analysis, in contrast to the conventional PCA, which is based on the additive model. At the same time, the variance can be discussed in terms of the additive model when ASIs are plotted in the log-scale.

Expressed mathematically, our approach leads to the following representation of measured angular scattering intensities $\sigma_j(\theta_i)$ in terms of the principal components $\xi_l(\theta_i)$, that is, the first k eigenvectors of the correlation matrix of the log-transformed data-set:

$$\ln\left[\sigma_j(\theta_i)\right] \approx \langle \ln[\sigma(\theta_i)] \rangle + \sum_{l=1}^{k} C_{j,l}\xi_l(\theta_i),$$

where θ_i is the scattering angle, the index i designates the i-th scattering angle and takes values from 1 to 32, the index j refers to the j-th observation of the analyzed flight sequences, <…> denotes averaging over the total data set (i.e., 1803 PN measurements). When vector expressions are employed, $\overrightarrow{\sigma_j}$ has the components $\sigma_j(\theta_i)$; $\overrightarrow{\xi_l}$, $\overrightarrow{\ln\sigma_j}$, and $\overrightarrow{\ln\sigma}$ have the components $\xi_l(\theta_i)$, $\ln\left[\sigma_j(\theta_i)\right]$, and $\langle \ln[\sigma(\theta_i)] \rangle$, respectively. The coefficients $C_{j,l}$ are computed as: $C_{j,l} = \left(\overrightarrow{\ln\sigma_j} - \langle\overrightarrow{\ln\sigma}\rangle\right)^T \cdot \overrightarrow{\xi_l}$, where ^{T} denotes a transposed matrix. Each vector (i.e., $\overrightarrow{\ln\sigma_j}$ at each j) is represented by a few coefficients $C_{j,l}$ with quite good accuracy.

3.2 Clustering results

The PCA results were obtained using the CONCERT data recorded during the flights on 16 September 2011 (from 14:40 to 17:50 UTC) (Kaufmann et al., 2014) and on 30 September 2011 (from 6:50 to 8:40 UTC) (Voigt et al., 2014a). The data set contains the ASIs measured in degassing plumes, cirrus and contrails. Such a large set was chosen to point out that the scattering pattern of degassing plumes is clearly distinctive (see below).

When the PCA is applied to ASIs, the principal components can have a clear physical meaning. Figure 3(a) shows the first three principal components along with the corresponding eigenvalues λ_l normalized as a percentage of the total variance. The first vector $\overrightarrow{\xi_1}$ almost does not depend on the scattering angle, it accounts for 96.8 % of the data variability. This means that it is closely linked to the extinction coefficient and about 97 % of the ASIs variation is mostly due to fluctuations of the particles concentration.

It is well known that effects of a size distribution, refractive index, particles shape, surface roughness, are better represented using phase functions, i.e., normalized ASIs. Thus, not only the other principal components are of importance, their contribution to the remaining variability has to be evaluated.

The second vector $\overrightarrow{\xi_2}$ represents 70.4% of the remaining variability; it has negative values at sideward angles. Generally, high negative values of the corresponding coefficients $C_{j,2}$ of such a vector take into account the irregular shape and/or the deep surface roughness of large particles. And, all of this leads to lower values of the asymmetry parameter (see, e.g., Jourdan et al., 2010).

The third vector $\overrightarrow{\xi_3}$ represents 15.6% of the remaining variability. Its shape reveals that $\overrightarrow{\xi_3}$ is related to the forward/backward-hemisphere partitioning of the scattering. The high negative values of the corresponding coefficients $C_{j,3}$ imply that less energy is scattered in the forward hemisphere and, thus, more energy is scattered in the backward hemisphere.

Figure 3(b) shows the scatterplot of the $C_{j,3}$ expansion coefficient versus the $C_{j,2}$ coefficient. Therefore, such a presentation describes the features of the PN data set in one of the clearest and informative ways. Each point is directly associated with one of the measured ASCs. Three main distinctive clusters of points can be identified in Fig. 3(b). Additional analysis of the total CONCERT-2011 data set provided possibility to associate the clusters with the measurements performed within cirrus clouds, contrails and the degassing volcanic plumes (see the notations in Figure 3(b)).

The negative $C_{j,2}$ values of the cirrus cluster are typical of irregular large ice particles (see, e.g., Jourdan et al., 2010). The contrails cluster is characterized by high positive values of $C_{j,2}$. This feature means that the corresponding phase functions are quite similar to those of ensembles of large spherical particles. The fraction of spherical particles increases with increasing $C_{j,2}$. This is especially true for the young-contrails sub-cluster. A detailed discussion can be found in Gayet et al. (2012).

The peculiarity of the degassing-plumes cluster is that the coefficients $C_{j,2}$ are close to zero. Thus, the properties of the degassing-plumes ASIs can be discussed just in terms of the vector $\overrightarrow{\xi_3}$. That fact results in the following. The effective diameter and the asymmetry parameter of the degassing-plumes particles have to be smaller, if not much smaller, compared to those ones of other clusters of the data set, among them the young contrails. Another property of the degassing-plumes cluster is that it falls into sub-clusters. Figure 3(c) repeats Fig. 3(b) but with the focus of attention on the degassing plumes. It is seen that the ASIs of the NECa and NECb plumes are close to each other; they form one cluster. The BNa and BNb clusters are a little bit separated with the third coefficients, but belong to the same range of the second coefficient that accounts for 70.4% of the ASIs shape variability. Other properties of the degassing-plumes sub-clusters will be discussed in details below.

4 Number concentrations, effective radii and refractive indices of the volcanic plume layers

In this work the intervals of the degassing-plume penetration were specified on the basis of the PN data after subtraction of the background signals, which correspond to the electronic noise and ASIs of the free atmosphere. The angular scattering intensities (ASI) from the Polar Nephelometer were averaged over the penetration intervals, i.e., over 17 seconds for Stromboli (SV) and over 143, 172, 122, 80 and 313 seconds for Etna's Bocca Nuova (BNa and BNb) and North East (NECa1, NECa2, and NECb) crater plumes, respectively (see notations in Fig. 1). The averaged ASIs were used to retrieve microphysical and optical characteristics of degassing-plumes aerosols.

4.1 Retrieval techniques and software

Our retrievals were performed with the software and the pre-calculated kernels developed by Dubovik et al. (2006). We recall that the software is employed in the operational processing of AERONET (AErosol RObotic NETwork) for retrieving detailed properties from observations of ground-based sun/sky-radiometers (Eck et al., 2008). We will briefly describe the main features of the retrieval algorithm and its implementation on our specific dataset.

The pre-calculated kernels contain optical characteristics of spheroids mixtures. The surface of particles can be smooth or severely rough (Yang et al., 2013). A mixture of spheroids of different aspect ratios, sizes and surface texture (smooth or severely rough) is employed as a generalized aerosol model (representing spherical, non-spherical, and mixed aerosols). The aspect-ratio values belong to the range (0.3 – 3.0); the surface-roughness parameter can take only two values 0.0 or 0.2.

The code offers the possibility to retrieve a complete set of aerosol parameters, including the complex refractive index and the size distribution. The aerosol size distribution is presented using size bins; and the size bins are formed with discrete logarithmically equidistant size values. As for size-distribution retrievals, the undoubted advantage of the Dubovik code consists in the fact that solutions are constrained to be non-negative, which significantly improves the quality of retrievals. The constraint is imposed through an elegant and well-founded approach, more specifically, the assumption of the log-normal distribution of measurement errors (see, e.g., Dubovik et al., 2011).

The code includes a quite large set of input parameters that is very advantageous for an experienced user. For example, different hypotheses of aerosol composition, among others, effects of the ultrafine fraction, can be tested. On the one hand, supervised retrievals are time consuming; on the other, one has the possibility to assure a high quality of retrievals. We list some criteria of the retrieval quality in the following. Final results are scarcely affected by small variations of input parameters. When the regularization-parameter value is chosen according to the "L-curve" method (see, e.g., Hansen, 1992), the retrieval residuals correspond to the measurement errors. In a generally non-linear case, a particular attention must be given to the verification whether the obtained solution corresponds to the global

minimum of an objective function. As for aerosol-characteristics retrievals, different starting values of the refractive index may be randomly tried.

Summarized, we modeled the degassing plumes as a mixture of two main particle fractions; one consists of spherical and one of non-spherical particles. Although aerosol particles were not ellipsoidal, we consider randomly oriented spheroids as a reasonable approximation of an ensemble of quite small non-spherical aerosols. In addition, we recall that we considered smooth and severely rough particles (Yang et al., 2013).

Details of the software package, we used in this works, as well as of the code application are described in the supplementary material. To summarize briefly, different initial guesses for the inversion code were performed on a multidimensional grid of the input parameters using a number of input files. The minimum and the maximum sizes of particles as well as the spherical/non-spherical partitioning ratio belong to the set of assessed parameters in addition to the refractive index and the size distribution.

4.2 Retrieval results

Three representative examples of retrievals are shown in Fig. 4. The corresponding time-sequences SV, BNa and NECb are identified in the time-series in Fig. 2 by shadowed areas. In Fig. 4 (a-c), the left panels display the particle size distributions measured with the FSSP-300 and FSSP-100 (solid lines) and the retrieved one (solid black circles). It should be pointed out that the FSSP measurements in Fig. 4 represent particle size distributions considering the size response to water droplets. Due to size response uncertainties linked to different refractive indexes and/or particle shape in plume aerosols (Pinnick and Auvermann, 1979; Dye and Baumgardner, 1984; Jaenicke and Hanusch, 1993; Febvre et al., 2012), the comparison with retrieved size distributions should only be considered as qualitative in Fig. 4. Despite these limitations, the FSSP data and the retrieved distributions reveal very similar features of the degassing-plumes aerosols, in particular the absence of large particles. The calibrated probe response of the specific FSSP adjusted to different refractive indexes is beyond the scope of this paper.

The size distribution was retrieved along with the refractive index $m = n + i\,\chi$ and the spherical/non-spherical partitioning ratio (SNR) of aerosol particles (see Table 1). In the following, the SNR defines the percentage in number of spherical particles relative to the total number of particles. Furthermore, the refractive index and the partitioning ratio are assumed to be constant over the full size range of the retrieved particle size distribution. We emphasize that the information content of the PN data is inadequate to retrieve size-dependent values of such parameters. In other words, variations of the shape and/or the refractive index of small particles lead to variations of the phase function that are lower than the PN measurement errors. Therefore, the refractive index and the partitioning ratio are assumed to be constant over the full size range.

The following results are especially noteworthy. The real part *n* of the refractive index belongs to the interval from 1.35 to 1.38; the aerosol particles were either non-absorbing or weakly absorbing; the SNR values are equal to 100 %, i.e., the best fits of the Polar Nephelometer data were obtained with the model of spherical particles (Table 1).

The assessed value of the maximal particles diameter is about 15 μm for the all degassing-plume penetrations (Fig. 4). That is, the size parameter of the probed aerosols is rather small (lower than 60 for the wavelength of 0.8 μm). This feature can explain the fact that all our retrieval results were very close for the both value of the surface-roughness parameter. The PN measurements are not sensitive enough to distinguish whether small particles have smooth or rough surface. In view of this result and the SNR values, the degassing-plume aerosols are assumed to be smooth spheres.

The right panels of Fig. 4 (a-c) represent the following data. The average scattering phase function (without normalization) measured by the Polar Nephelometer is shown by solid red circles (see the averaging time intervals in Table 1). The retrieved phase function, shown by solid black circles, was computed from the retrieved size distribution. The main result of Fig. 4 is that the retrieved phase functions agree well with the observations. And, it should be underscored that there is no systematic bias between them. In other words, the measured ASIs are well fitted by the retrieved phase functions. The residuals *Res* were computed with the formula

$$Res = 100 \cdot \sqrt{\frac{1}{N}\sum_{i=1}^{N}\left[\frac{I(\theta_i)_{ret} - I(\theta_i)_{meas}}{I(\theta_i)_{meas}}\right]^2},$$

where $I(\theta_i)$ is the light intensity at the scattering angle θ_i, and the subscripts "*meas*" and "*ret*" refer to the measured and retrieved values, respectively. The low values of the residuals are noteworthy as well, see Table 1.

Table 1 summarizes the measured and retrieved characteristics. As mentioned above, the relative humidity RH_w was low, i.e., about 36 % within the Stromboli plume and near 10 % during the Etna plume samplings. The air temperature was positive, including at the Etna upper-plume altitude (0.3°C). The number concentration (*Conc*) of aerosols with the diameter $d > 0.9$ μm is estimated within the range of 25 – 51 cm^{-3}. The effective diameter (*Deff*) was low, between 1.5 and 2.8 μm, where both parameters *Conc* and *Deff* were deduced from the FSSP data. The retrieved values of the refractive index belong to the interval from 1.35 to 1.38. Low values [0.65 – 0.70] of the asymmetry parameter *g* correspond to ensembles of small particles, which is in agreement with the *Deff* values. The extinction coefficients *Ext* were computed form the retrievals data, the values are quite small confirming that the ASIs were recorded in single-scattering conditions. We recall that the optical characteristics correspond to the wavelength of 0.8 μm and that the all parameters were recorded at distances more than 6 km from the plumes sources.

As it was mentioned above, the ASIs of the degassing plumes are partitioned into sub-clusters (see Fig. 3c). The ASIs of the NECa and NECb plumes are spread within a cluster that is well distinguished from

other ones. The second coefficients $C_{j,2}$ of the BNa and BNb data are within the same range of values. (We recall that the second vector $\overrightarrow{\xi_2}$ represents 70.4% of the ASIs shape variability.) Consequently, the asymmetry-parameter values of the Bocca Nuova plumes (BNa and BNb) are a little bit higher compared to those ones of the North East crater (NECa1, NECa2, NECb), see Table 1. The histograms in Fig. 5 show probability distribution functions of the asymmetry-parameter values computed from the measured ASIs of the BNa and NECb plumes. These two distributions were selected only by reason of larger data sets, i.e., higher statistical significance. Generally speaking, the BNb and NECa distributions are close to histograms of the BNa and NECb, respectively. As it is seen on Fig. 5, the distributions are narrow suggesting quite homogeneous aerosol-plumes properties. The distinction between optical characteristics of the BN and NEC plumes could result from the difference in chemical composition of aerosols (Voigt et al., 2014a). Though completely independent, this classification of the individual volcanic plumes is similar to results from trace gas composition measurements of Voigt et al., (2014a) for plumes SV, BNb, NECa and NECb. In addition, the difference in the BN and NEC aerosol emissions was underscored earlier by Allen et al. (2006), who studied aerosol particles at the summit of Mt. Etna downwind from the degassing vents, and by Scollo et al. (2012), who reported observations of the Multi-angle Imaging SpectroRadiometer. Martin et al., (2008) evidenced persistent differences in the size distributions of sulfate aerosols between the two main Etna summit plumes.

5 Discussion and inferences

Our results in Table 1 show that the spherical/non-spherical partitioning ratio (SNR) value is of 100% for the all considered cases of degassing plumes. In other words, the best fits of the Polar Nephelometer data were obtained with the model of spherical aerosol-particles. It must be emphasized that this result does not mean that aerosols were perfect spheres. Since (i) the aerosol-particles were quite small with respect to the wavelength of 0.8 μm (see the effective-diameter values in Table 1), (ii) the angular scattering intensities (ASIs) were measured within the limited range of angles for the relatively small number of θ_i, (iii) the ASIs were averaged over an ensemble of particles, and (iv) the PN data were affected by measurement errors, we only can conclude that the aerosols of the degassing plumes were "optically spherical" (see, e.g., Dick et al., 1998). The term "optically spherical" should be considered within the context of optical instrumentation. For example, the model of spherical particles matches well the PN experimental data; and we believe that the asymmetry-parameter estimates are trustworthy. At the same time, it might be that polarization measurements, particularly in the backward hemisphere, will reveal non-spherical features of degassing-plumes aerosols.

The retrievals indicate that the aerosol particles were either non-absorbing or weakly absorbing with an upper bound for the imaginary part of the refractive index of 10^{-4}. Variations of the phase functions for

the imaginary part within the interval [0; 10^{-4}] are smaller than the measurement errors (Verhaege et al., 2008).

The most important and somewhat unexpected result of this work is the fact that the retrieved values of the real part *n* of the refractive index belong to the interval from 1.35 to 1.38 (Table 1).

Degassing-plumes aerosols of Mt. Etna were probed at distances greater than 6 km from the sources, i.e., the volcanic craters. The recorded values of the horizontal air-speed at the flight altitudes were 5.9 m/s or lower. Consequently, our measurements are related to aerosols that were generated more than 16.5 minutes before. Large aerosols tend to settle quickly out of the atmosphere. High initial concentrations of fine particles decay rapidly in the atmosphere due to coagulation and dilution, so that measurements depend on the distance from the source and the wind conditions (Ammann and Burtscher, 1990). Thus, it is hardly possible to directly compare our *in situ* data and characteristics of particles sampled on filters at the ground. Nevertheless, some ideas on the chemical composition of degassing-plumes aerosols can be drawn from published results.

Electron-microscopy analysis of particles in the range of diameters 5 – 100 nm showed significant levels of silicate nanoparticles in the Mt. Etna plumes (Ammann and Burtscher, 1990; Martin et al., 2008). As it was mentioned above, the Dubovik code provides possibility to evaluate effects of the ultrafine fraction, i.e., nanoparticles, on retrieval results. Our simulations and tests led us to the following conclusions. The information content of the PN data is inadequate for a correct estimation of the ultrafine-fraction number-concentration. Variations of that number concentration within a large range of values do not affect the retrieved values of the refractive index.

According to chromatographic analysis of ionic species of soluble particles sampled on filters from degassing plumes near the crater rims of Mt. Etna (Allen et al., 2006; Martin et al., 2008), aerosols are mainly composed of sulfates. Fluorides, chlorides and nitrates are present as well. Besides, silicates were observed in Etna degassing plumes (Lefevre et al., 1986; Martin et al., 2008). Generally, the values of the bulk refractive index at λ=0.8 μm of sulfates and other soluble inorganic species presumed to form the degassing plumes belong to the interval 1.48 – 1.58 or higher (see, e.g., Toon et al., 1976; Tang, 1996; Lide, 2010). The exception is some alkali halides with *n* about 1.40 or lower. For example, the refractive index values at λ=0.8 μm of NaF, KF, and MgF2 are 1.323, 1.36, and 1.375, respectively (Li, 1976). As for silicate particles, they have quite large values of the bulk refractive index, e.g., *n* is about 1.46 for amorphous silica glass (see, e.g., Kitamura et al., 2007), 1.52 – 1.59 or higher for feldspars (Lide, 2010), and about 1.56 – 1.99 or higher for garnets and other silicate minerals (Lide, 2010).

It is obvious that the retrieved values *n* (Table 1) are substantially lower than the bulk refractive index of sulfates and other inorganic matter presumed to form the degassing plumes. That result was thoroughly verified. The Dubovik code provides possibility to hold fixed a refractive-index value n_{fix} while a size distribution is retrieved, and to compute scattering characteristics for given optical

constants and the retrieved size distribution. As it is expected, the residuals *Res* increased when the fixed value n_{fix} of the refractive index deviated from the retrieved one. Two important points are to be underscored. When n_{fix} was higher than 1.40, (i) the *Res* values significantly exceeded the measurement-errors level; (ii) the plots of the reconstructed angular scattering coefficients, that is, computed for n_{fix} and the corresponding size distribution, clearly manifested a systematic deviation from the plots of the measured ASIs. An illustration of the systematic deviation is given in Fig. 6. The phase functions, i.e., the normalized ASIs, were computed for the retrieved size distribution of the NECb case (see Fig. 4) and a set of values of the real part *n* of the refractive index. It is seen that the behaviour of the curves within the scattering-angles interval of 15 – 150 degrees is sensitive to the *n* value. Not only the slopes of the curves are different but the local minimum shifts monotonically from 114° (*n*=1.33) to 124° (*n*=1.58). The gray bar in Fig. 6 indicates the range of the PN operating angles. Thus, we can say that the accuracy of the refractive-index estimation is based on the functional behaviour of measured ASIs. That conclusion corroborates the results of sensitivity tests performed by Verhaege et al., (2008) for ASIs measured within a limited range of scattering angles. It was shown that despite the absence of aureole and backward measurements the real part of the refractive index and the microphysical parameters can be retrieved in the case of the low absorbing particles.

It is unlikely that the relative concentration of alkali halides increased at distances greater than 6 km from the sources so that their optical properties became dominant. And in our particular case, the hypothesis of aqueous solutions or suspensions in the Mt. Etna plumes has to be rejected as well because of the very low relative humidity at the flight altitudes (Table 1). The measured RH_w values (about 10%) are much lower than the efflorescence RH_w of the overwhelming majority of the mentioned above chemical species (see, e.g., Table 3, Martin, 2000). We recall that efflorescence is a specific process in the more encompassing concept of crystallization, it specifically involves water vapor (Martin, 2000). In other words, the conditions were favorable even for homogeneous nucleation. As for the chemical systems $NaNO_3/H_2O$, NH_4HSO_4/H_2O, and NH_4NO_3/H_2O that do not readily crystallize at the lowest RH_w values (Martin, 2000), the conditions were favorable for heterogeneous nucleation due to significant levels of silicate nanoparticles in the Mt. Etna plumes (Martin et al., 2008). The hypothesis of unsteady state conditions was discarded in view of the data of the PCA analysis. For example, NECb plume was probed at distances from the craters between 5.9 and 47.7 km, respectively. Such distances correspond to the aerosol age between 16.5 minutes and two hours. There is no trend in *g* values of the NECa plume. A slight rise at the end of the NECb *g* series may be due to increased measurement errors at low aerosol concentrations.

In view of the results above, the most reasonable conclusion to make is that the aerosol particles of the degassing plumes were porous with air voids. Therefore, the retrieved values *n* (Table 1) correspond to the refractive index of the effective medium instead of the bulk one.

That conclusion is in agreement with data of transmission electron microscopy of aerosol particles collected in the remote marine troposphere (Pósfai et al., 1999). Figure 3(a) by Pósfai et al. (1999) is especially noteworthy. It shows a quasi-spherical ammonium-sulfate aerosol particle of about 1 μm diameter. The particle has the onion-like structure with soot inclusions. Obenholzner et al., (2003) investigated the micro-morphology of aerosol particles from the passively degassing plume of Popocatepetl volcano using the Field emission scanning electron microscopy (FESEM). A large set of spherical particles were observed; including spongy, i.e., porous aerosols and spheres, enclosing a dozen small crystals Obenholzner et al., (2003). Moreover, porosity could be the cause of the quite low values of the refractive index of the Eyjafjallajökull volcanic aerosol retrieved from POLDER/PARASOL measurements (Waquet et al., 2014).

Microwave analog experiments performed by Kolokolova and Gustafson, (2001) corroborate our conclusion as well. The measured ASIs of inhomogeneous particles show reasonable agreement with effective medium approximations (Kolokolova and Gustafson, 2001). The effective-medium approximation (EMA) along with the Maxwell Garnett mixing rule have already been used in a number of works to calculate optical properties of porous particles (see, e.g., Voshchinnikov et al., 2007; Kylling et al., 2014). The question of EMA applicability is discussed in details by Mishchenko et al., 2016.

At the wavelength of 0.8 μm, the real part of the bulk refractive index of sulfates, nitrates and other inorganic matter presumed to form the degassing plumes belongs to the range about 1.48 – 1.58. As for the imaginary part χ, it is very small, i.e. lower than 10^{-6} at the wavelength of 0.8 μm (see, e.g., Gosse et al., 1997). We recall that the aerosol particles are found to be either non-absorbing or weakly absorbing according to our retrievals. Thus, we assumed that $\chi=0.0$ in the following estimations.

Considering the range of [1.48 – 1.58], we employed the Maxwell Garnett mixing rule (Maxwell Garnett, 1904; see also Kolokolova and Gustafson, 2001) to estimate the volume fraction f of the inorganic matter that leads to the refractive index of the mixture about [1.35 – 1.38]. In other words, the inorganic matter and the air voids were taken as the matrix and the inclusions, respectively. We have obtained the interval of [0.65 – 0.82] as the estimate for the volume-fraction value. This means that aerosol particles of the degassing plumes contained 18 – 35 % of air voids (in terms of the total volume). The estimated volume fraction f and the bulk-refractive-index range of inorganic matter would lead to the refractive index of aerosols about [1.43 – 1.53] if pores were filled up with water. The last assessment is in agreement with the results by Waquet et al., (2014).

Our finding has the following consequences. (i) Climate models, optical methods of remote sensing and optical instruments of particles counting have to consider not the bulk- but the effective refractive index of volcanic particles and aerosols in general. (ii) The volume fraction f of bulk matter has to be taken into account in assessing the volcanic ash spreading and loading. (iii) The volume fraction f has to be

considered in aerosols sizing instrumentation based on the inertial separation. (iv) Aerosols porosity could be of importance for condensation and freezing processes.

6 Conclusions

Volcanic degassing plumes were probed on 30 September 2011 with *in situ* instruments onboard the DLR Falcon research aircraft during the CONCERT experiment. The plumes were spreading in the dry troposphere at temperatures above the freezing point.

Aerosols of degassing plumes from the volcanoes Mt. Etna and Mt. Stromboli are characterized by quite low values of the asymmetry parameter (between 0.6 and 0.75); their scattering features are clearly distinctive from angular scattering intensities of cirrus and contrails.

The measured and the retrieved size distributions of the degassing-plumes aerosols are in good agreement. The effective diameter of the aerosols was within the range of 1.5 – 2.8 µm, the maximal diameter of particles was lower than 20 µm.

Retrievals of aerosol properties revealed that the particles were "optically spherical"; the estimated values of the real part of the refractive index belong to the interval from 1.35 to 1.38, which is substantially lower than the bulk refractive index of sulfates, nitrates and other inorganic matter presumed to form the degassing plumes.

That property leads to the conclusion that the aerosol particles of the degassing plumes were porous with air voids. Our estimates, based on the Maxwell Garnett mixing rule, suggest that aerosol particles of the degassing plumes contained 18 – 35 % of air voids in terms of the total volume.

Acknowledgments

We thank the DLR flight department for excellent support during the CONCERT campaign. The campaign was organized by the Research Group AEROTROP under HGF contract VH-NG-309. Part of this work is funded by the Research Cluster VAMOS at Johannes Gutenberg University, Mainz and by the German Science Foundation DFG within SPP1294 HALO. J.-F. Gayet is grateful to DLR for having provided a guest scientist opportunity at the Institut für Physik der Atmosphäre during this study.

References

Abo Riziq, A., Erlick, C., Dinar, E., and Rudich, Y.: Optical properties of absorbing and non-absorbing aerosols retrieved by cavity ring down (CRD) spectroscopy, Atmos. Chem. Phys., 7, 1523-1536, doi:10.5194/acp-7-1523-2007, 2007.

Adler, G., T. Koop, C. Haspel, I. Taraniuk, T. Moise, I. Koren, R. H. Heiblum, and Y. Rudich: Formation of highly porous aerosol particles by atmospheric freeze-drying in ice clouds, Proc. Natl. Acad. Sci. U.S.A., doi:10.1073/pnas.1317209110, 2013.

Adler, G., C. Haspel, T. Moise, and Y. Rudich: Optical extinction of highly porous aerosol following atmospheric freeze drying, J. Geophys. Res. Atmos., 119, 6768–6787, doi:10.1002/2013JD021314, 2014.

Allen, A. G., T. A. Mather, A. J. S. McGonigle, A. Aiuppa, P. Delmelle, B. Davison, N. Bobrowski, C. Oppenheimer, D. M. Pyle, and S. Inguaggiato, Sources, size distribution, and downwind grounding of aerosols from Mount Etna, J. Geophys. Res. Atmos., 111, D10302, doi:10.1029/2005JD006015, 2006.

Ammann, M., Burtscher, H.: Characterization of ultrafine aerosol particles in Mt. Etna emissions, Bull. Volcanol., 52, 577–583, doi:10.1007/BF00301209, 1990.

Baumgardner, D., J. E. Dye, B. W. Gandrup, and R. G. Knollenberg: Interpretation of measurements made by the Forward Scattering Spectrometer Probe (FSSP-300) during the Airborne Arctic Stratosphere Expedition, J. Geophys. Res. Atmos., 97, 8035–8046, doi:10.1029/91JD02728, 1992.

Chýlek, P., Srivastava, V., Pinnick, R G., and Wang, R.: Scattering of electromagnetic waves by composite spherical particles: Experiment and effective medium approximation, Appl. Opt., 27, 2396–2404, doi:10.1364/AO.27.002396, 1988.

Chýlek, P., Videen, G., Geldart, D. J. W., Dobbie, J. S., and Tso, H. C. W.: Effective medium approximations for heterogeneous particles, in: Light scattering by nonspherical particles, theory, measurements, and applications, edited by: Mishchenko, M. I., Hovenier, J. W., and Travis, L. D., Academic Press, 273–308, 2000.

Delmelle, P.: Environmental impacts of tropospheric volcanic gas plumes, in: Volcanic degassing, edited by: Oppenheimer, C., Pyle, D. M., and Barclay, J., Geol Soc London Special Publ, 213, 381–399, doi:10.1144/GSL.SP.2003.213.01.23, 2003.

Dick, W. D., Paul J Ziemann, Po-Fu Huang and Peter H McMurry: Optical shape fraction measurements of submicrometre laboratory and atmospheric aerosols, Meas. Sci. Technol., 9, 183–196, doi:10.1088/0957-0233/9/2/006, 1998.

Dubovik, O., A. Sinyuk,T. Lapyonok, B. N. Holben, M. Mishchenko, P. Yang, T. F. Eck, H. Volten, O. Muñoz, B. Veihelmann, W. J. van der Zande, J-F Leon, M. Sorokin, and I. Slutsker: Application of spheroid models to account for aerosol particle nonsphericity in remote sensing of desert dust, J. Geophys. Res. Atmos., 111, D11208, doi:10.1029/2005JD006619, 2006.

Dubovik, O., Herman, M., Holdak, A., Lapyonok, T., Tanré, D., Deuzé, J. L., Ducos, F., Sinyuk, A., and Lopatin, A.: Statistically optimized inversion algorithm for enhanced retrieval of aerosol properties from spectral multi-angle polarimetric satellite observations, Atmos. Meas. Tech., 4, 975–1018, doi:10.5194/amt-4-975-2011, 2011.

Dye, J. E. and Baumgardner, D.: Evaluation of the forward scattering spectrometer probe, I – Electronic and optical studies, J. Atmos. Ocean. Tech., 1, 329–344, doi:10.1175/1520-0426(1984)001<0329:EOTFSS>2.0.CO;2, 1984.

Eck, T. F., B. N. Holben, J. S. Reid, A. Sinyuk, O. Dubovik, A. Smirnov, D. Giles, N. T. O'Neill, S.-C. Tsay, Q. Ji, A. Al Mandoos, M. Ramzan Khan, E. A. Reid, J. S. Schafer, M. Sorokine, W. Newcomb, and I. Slutsker: Spatial and temporal variability of column-integrated aerosol optical properties in the southern Arabian Gulf and United Arab Emirates in summer, J. Geophys. Res. Atmos., 113, D01204, doi:10.1029/2007JD008944, 2008.

Febvre G., Gayet J.-F., Shcherbakov V., Gourbeyre C., Jourdan, O.: Some effects of ice crystals on the FSSP measurements in mixed phase clouds, Atmos. Chem. Phys., 12, 8963–8977, doi:10.5194/acp-12-8963-2012, 2012.

Frey, W., S. Borrmann, D. Kunkel, R. Weigel, M. de Reus, H. Schlager, A. Roiger, C. Voigt, P. Hoor, J. Curtius, M. Krämer, C. Schiller, C. M. Volk, C. D. Homan, F. Fierli, G. Di Donfrancesco, A. Ulanovsky, F. Ravegnani, N. M. Sitnikov, S. Viciani, F. D'Amato, G. Shur, G. V. Belyaev, K. Law, and F. Cairo: In situ measurements of tropical cloud properties in the West African Monsoon: upper tropospheric ice clouds, Mesoscale Convective System outflow, and subvisual cirrus, Atmos. Chem. Phys., 11, 5569–5590, doi:10.5194/acp-11-5569-2011, 2011.

Fulignati P., A. Sbrana, R. Clocchiatti, and W. Luperini: Environmental impact of the acid fumarolic plume of a passively degassing volcano (Vulcano Island, Italy), Environ. Geol., 49, 8, 1139–1155, doi:10.1007/s00254-005-0158-0, 2006.

Gayet, J.-F., Crépel, O., Fournol, J.-F., and Oshchepkov, S.: A new airborne polar Nephelometer for the measurements of optical and microphysical cloud properties. Part I: Theoretical design, Ann. Geophys., 15, 451–459, doi:10.1007/s00585-997-0451-1, 1997.

Gayet, J.-F., S. Asano, A. Yamazaki, A. Uchiyama, A. Sinyuk, O. Jourdan, and F. Auriol: Two case studies of winter continental-type water and mixed-phase stratocumuli over the sea: 1. Microphysical and optical properties, J. Geophys. Res., 107(D21), 4569, doi:10.1029/2001JD001106, 2002.

Gayet, J.-F., Shcherbakov, V., Voigt, C., Schumann, U., Schäuble, D., Jessberger, P., Petzold, A., Minikin, A., Schlager, H., Dubovik, O., and Lapyonok, T.: The evolution of microphysical and optical properties of an A380 contrail in the vortex phase, Atmos. Chem. Phys., 12, 6629–6643, doi:10.5194/acp-12-6629-2012, 2012.

Gosse, S. F., M. Wang, D. Labrie, and P. Chylek: Imaginary part of the refractive index of sulfates and nitrates in the 0.7–2.6 μm spectral region, Appl. Opt., 36(16), 3622–3634, doi:10.1364/AO.36.003622, 1997.

Hansen, P. C.: Analysis of discrete ill-posed problems by means of the L-curve, SIAM Rev., 34, 561–580, doi:10.1137/1034115, 1992.

Heiken, G., and K. Wohletz: Volcanic Ash, Univ. of Calif. Press, Berkeley, 246 pp., 1985.

Jeßberger, P., Voigt, C., Schumann, U., Sölch, I., Schlager, H., Kaufmann, S., Petzold, A., Schäuble, D., and Gayet, J.-F.: Aircraft type influence on contrail properties, Atmos. Chem. Phys., 13, 11965–11984, doi:10.5194/acp-13-11965-2013, 2013.

Jaenicke, R., and Hanusch, T.: Simulation of the Optical Particle Counter Forward Scattering Spectrometer Probe 100 (FSSP-100), Aerosol Sci. Tech., 18, 4, 309–322, doi:10.1080/02786829308959607, 1993.

Jeong, G. Y. and Nousiainen, T.: TEM analysis of the internal structures and mineralogy of Asian dust particles and the implications for optical modeling, Atmos. Chem. Phys., 14, 7233–7254, doi:10.5194/acp-14-7233-2014, 2014.

Johnson, R. A., and Wichern, D. J.: Applied multivariate statistical analysis, 4th ed., Prentice hall Inc, New Jersey, 816 pp., 1998.

Jolliffe I. T.: Principal Component Analysis, Series: Springer Series in Statistics, 2nd ed., Springer, NY, 487 p., 2002.

Jourdan O., S. Oshchepkov, J-F Gayet, V. Shcherbakov and H. Isaka: Statistical analysis of cloud light scattering and microphysical properties obtained from airborne measurements. J. Geophys. Res., 108, D5, doi:10.1029/2002JD002723, 2003.

Jourdan O., G. Mioche, T. J. Garret, A. Schwarzenbock, J. Vidot, Y. Xie, V. Shcherbakov, C. Duroure, P. Yang and J.-F. Gayet: Coupling of the microphysical and optical properties of arctic clouds during the ASTAR 2004 experiment: Implications for light scattering modelling, J. Geophys. Res.,115, doi:10.1029/2010JD014016, 2010.

Jurkat, T., C. Voigt, F. Arnold, H. Schlager, H. Aufmhoff, J. Schmale, J. Schneider, M. Lichtenstern and A. Dörnbrack: Airborne stratospheric ITCIMS-measurements of SO2, HCl, and HNO3 in the aged plume of volcano Kasatochi, J. Geophys. Res., 115, D00L17, doi:10.1029/2010JD013890, 2010.

Jurkat, T., C. Voigt, F. Arnold, H. Schlager, J. Kleffmann, H. Aufmhoff, D. Schäuble, M. Schaefer, and U. Schumann: Measurements of HONO, NO, NO_y and SO_2 in aircraft exhaust plumes at cruise, Geophys. Res. Lett., 38, L10807, doi:10.1029/2011GL046884, 2011.

Jurkat, T., Kaufmann, S., Voigt, C., Schäuble, D., Jeßberger, P., and Ziereis, H.: The airborne mass spectrometer AIMS – Part 2: Measurements of trace gases with stratospheric or tropospheric origin in the UTLS, Atmos. Meas. Tech., 9, 1907-1923, doi:10.5194/amt-9-1907-2016, 2016.

Kahn, R. A., W.-H. Li, C. Moroney, D. J. Diner, J. V. Martonchik, and E. Fishbein: Aerosol source plume physical characteristics from space-based multiangle imaging, J. Geophys. Res., 112, D11205, doi:10.1029/2006JD007647, 2007.

Kaufmann, S., C. Voigt, P. Jeßberger, T. Jurkat, H. Schlager, A. Schwarzenboeck, M. Klingebiel, and T. Thornberry: In situ measurements of ice saturation in young contrails, Geophys. Res. Lett., 41, 702–709, doi:10.1002/2013GL058276, 2014.

Kaufmann, S., Voigt, C., Jurkat, T., Thornberry, T., Fahey, D. W., Gao, R.-S., Schlage, R., Schäuble, D., and Zöger, M.: The airborne mass spectrometer AIMS – Part 1: AIMS-H_2O for UTLS water vapor measurements, Atmos. Meas. Tech., 9, 939–953, doi:10.5194/amt-9-939-2016, 2016.

Kitamura, R., L. Pilon, and M. Jonasz: Optical constants of silica glass from extreme ultraviolet to far infrared at near room temperature, Appl. Opt., 46, 8118–8133, doi:10.1364/AO.46.008118, 2007.

Kolokolova L., and Gustafson, B.A.S.: Scattering by inhomogeneous particles: microwave analog experiments and comparison to effective medium theories, J. Quant. Spectrosc. Ra., 70, 611–25, doi:10.1016/S0022-4073(01)00033-4, 2001.

Kylling, A., Kahnert, M., Lindqvist, H., and Nousiainen, T.: Volcanic ash infrared signature: porous non-spherical ash particle shapes compared to homogeneous spherical ash particles, Atmos. Meas. Tech., 7, 919-929, doi:10.5194/amt-7-919-2014, 2014.

Lefevre, R., A. Gaudichet, and M. A. Billongalland: Silicate microspherules intercepted in the plume of Etna volcano, Nature, 322, 817 – 820, doi:10.1038/322817a0, 1986.

Li, H. H,: Refractive index of alkali halides and its wavelength and temperature derivatives, J. Phys. Chem. Ref. Data, 5, 329–528 doi:10.1063/1.555536, 1976.

Lide, D. R. (Ed.): CRC Handbook of Chemistry and Physics 90th Edition, CRC Press, 2010.

Liu C., R. Lee Panetta, and P. Yang: Inhomogeneity structure and the applicability of effective medium approximations in calculating light scattering by inhomogeneous particles, J. Quant. Spectrosc. Ra., 146, 331–348, doi:10.1016/j.jqsrt.2014.03.018, 2014.

Marenco, F., B. Johnson, K. Turnbull, S. Newman, J. Haywood, H. Webster, and H. Ricketts: Airborne lidar observations of the 2010 Eyjafjallajökull volcanic ash plume, J. Geophys. Res., 116, D00U05, doi:10.1029/2011JD016396, 2011.

Martin, R. S., T. A. Mather, D. M. Pyle, M. Power, A. G. Allen, A. Aiuppa, C. J. Horwell, and E. P. W. Ward: Composition-resolved size distributions of volcanic aerosols in the Mt. Etna plumes, J. Geophys. Res., 113, D17211, doi:10.1029/2007JD009648, 2008.

Martin, R. S., T. A. Mather, D. M. Pyle, M. Power, V. I. Tsanev, C. Oppenheimer, A. G. Allen, C. J. Horwell, and E. P. W. Ward: Size distributions of fine silicate and other particles in Masaya's volcanic plume, J. Geophys. Res., 114, D09217, doi:10.1029/2008JD011211, 2009.

Martin, S. T.: Phase transitions of aqueous atmospheric particles, Chem. Rev., 100, 3403–3454, doi:10.1021/cr990034t, 2000.

Mather, T.A., Pyle, D.M. and Oppenheimer, C.: Tropospheric Volcanic Aerosol, in: Volcanism and the Earth's Atmosphere, edited by: Robock, A., and Oppenheimer, C., American Geophysical Union, Washington, D. C.. doi:10.1029/139GM12, 2004.

Maxwell Garnett, J. C.: Colours in metal glasses and in metallic films, Philos Trans Roy Soc A 203, 385–420, doi:10.1098/rsta.1904.0024, 1904.

Mishchenko, M.I., L.D. Travis, R.A. Kahn, and R.A. West: Modeling phase functions for dustlike tropospheric aerosols using a mixture of randomly oriented polydisperse spheroids, J. Geophys. Res., 102, 16831–16847, doi:10.1029/96JD02110, 1997.

Mishchenko, M. I., Wiscombe, W. J., Hovenier, J. W. and Travis, L. D.: Overview of scattering by nonspherical particles, in: Light Scattering by Nonspherical Particles, edited by: Mishchenko, M. I., Hovenier, J. W. and Travis, L. D., Academic Press, San Diego, CA, USA, Chap. 2, 29–60, 2000.

Mishchenko, M.I., Dlugach, J.M., Yurkin, M.A., Bi, L., Cairns, B., Liu, L., Panetta, R.L., Travis, L.D., Yang, P., and Zakharova, N.T.: First-principles modeling of electromagnetic scattering by discrete and discretely heterogeneous random media, Phys. Rep., 632, 1–75, doi:10.1016/j.physrep.2016.04.002, 2016.

Nousiainen, T.: Optical modeling of mineral dust particles: A review. J. Quant. Spectrosc. Ra., 110, 1261–1279, doi:10.1016/j.jqsrt.2009.03.002, 2009.

Obenholzner, J. H., Schroettner, H., Golob, P.and Delgado, H.: Particles from the plume of Popocatepetl volcano, Mexico - the FESEM/EDS approach, in: Volcanic degassing, edited by: Oppenheimer, C., Pyle, D. M., and Barclay, J., Geol Soc London Special Publ, 213, 123–148, doi: 10.1144/GSL.SP.2003.213.01.08, 2003.

Oppenheimer, C., Scaillet, B., and Martin, R. S.: Sulfur degassing from volcanoes: source conditions, surveillance, plume chemistry and Earth system impacts, Rev. Mineral. Geochem., 73, 363–421, doi:10.2138/rmg.2011.73.13, 2011.

Petzold, A., Busen, R., Schröder, F. P., Baumann, R., Kuhn, M., Ström, J., Hagen, D. E., Whitefield, P. D., Baumgardner, D., Arnold, F., Borrmann, S., and Schumann, U.: Near-field measurements on contrail properties from fuels with different sulfur content, J. Geophys. Res., 102, 29867–29880, doi: 10.1029/97JD02209, 1997.

Pinnick R.G., and Auvermann, H. J.: Response Characteristics of Knollenberg Light-Scattering Aerosol Counters, J. Aerosol Sci., 10, 55-74, doi:10.1016/0021-8502(79)90015-6, 1979.

Pósfai, M., Anderson, J.R., Buseck, P.R., and Sievering, H.: Soot and sulfate aerosol particles in the remote marine troposphere, J. Geophys. Res., 104:21685–21693, doi:10.1029/1999JD900208, 1999.

Schmidt, A., Carslaw, K. S., Mann, G. W., Rap, A., Pringle, K. J., Spracklen, D. V., Wilson, M., and Forster, P. M.: Importance of tropospheric volcanic aerosol for indirect radiative forcing of climate, Atmos. Chem. Phys., 12, 7321-7339, doi:10.5194/acp-12-7321-2012, 2012.

Scollo, S., R. A. Kahn, D. L. Nelson, M. Coltelli, D. J. Diner, M. J. Garay, and V. J. Realmuto, MISR observations of Etna volcanic plumes, J. Geophys. Res., 117, D06210, doi:10.1029/2011JD016625, 2012.

Shcherbakov V., J.-F. Gayet, O. Jourdan, A. Minikin, J. Ström and A. Petzold: Assessment of cirrus cloud optical and microphysical data reliability by applying statistical procedures, J. Atmos. Oceanic. Technol., 22, 409-420, doi:10.1175/JTECH1710.1, 2005.

Shcherbakov V., Gayet, J.-F., Baker, B.A., and Lawson, R.P.: Light scattering by single natural ice crystals, J Atmos Sci, 63, 1513–1525, doi:10.1175/JAS3690.1, 2006.

Spinetti, C., M. F. Buongiorno, V. Lombardo, and L. Merucci: Aerosol optical thickness of Mt. Etna volcanic plume retrieved by means of the Airborne Multispectral Imaging Spectrometer (MIVIS), Ann. Geophys., 46, 2, 439–449, doi:10.4401/ag-3417, 2003.

Tang, I. N.: Chemical and size effects of hygroscopic aerosols on light scattering coefficients, J. Geophys. Res., 101, 19245–19250, doi:10.1029/96JD03003, 1996.

Tang, I. N., and Munkelwitz, H. R.: Simultaneous Determination of Refractive Index and Density of an Evaporating Aqueous Solution Droplet, Aerosol Sci. Tech., 15, 3, 201-207, doi:10.1080/02786829108959527, 1991.

Toledano, C., Bennouna, Y., Cachorro, V., Ortiz de Galisteo, J. P., Stohl, A., Stebel, K., Kristiansen, N. I., Olmo, F. J., Lyamani, H., Obregón, M. A., Estellés, V., Wagner, F., Baldasano, J. M., González-Castanedo, V, Clarisse, L., and de Frutos, A. M.: Aerosol properties of the Eyjafjallajökull ash derived from sun photometer and satellite observations over the Iberian Peninsula, Atmos. Environ., 48, 22–32, doi:10.1016/j.atmosenv.2011.09.072, 2012.

Toon, O. B., Pollack, J. B., and Khare, B. N.: The optical constants of several atmospheric aerosol species: ammonium sulfate, aluminum oxide, and sodium chloride, J. Geophys. Res., 81, 5733–5748, doi:10.1029/JC081i033p05733, 1976.

Ulanowski, Z., and Schnaiter, M.: UV and visible light scattering and absorption measurements on aerosols in the laboratory, in: Fundamentals and Applications of Aerosol Spectroscopy, edited by: Reid, J. P., and Signorell, R., CRC Press, Boca Raton, 243–268, doi:10.1201/b10417-14, 2011.

Verhaege, C., V. Shcherbakov, and P. Personne: Limitations on retrieval of complex refractive index of spherical particles from scattering measurements, J. Quant. Spectrosc. Ra., 109, 2338-2348, doi:10.1016/j.jqsrt.2008.05.009, 2008.

Voigt, C., Schumann, U., Jurkat, T., Schäuble, D., Schlager, H., Petzold, A., Gayet, J.-F., Krämer, M., Schneider, J., Borrmann, S., Schmale, J., Jessberger, P., Hamburger, T., Lichtenstern, M., Scheibe, M., Gourbeyre, C., Meyer, J., Kübbeler, M., Frey, W., Kalesse, H., Butler, T., Lawrence, M. G., Holzäpfel, F., Arnold, F., Wendisch, M., Döpelheuer, A., Gottschaldt, K., Baumann, R., Zöger, M., Sölch, I., Rautenhaus, M., and Dörnbrack, A.: In situ observations of young contrails – overview and selected results from the CONCERT campaign, Atmos. Chem. Phys., 10, 9039–9056, doi:10.5194/acp-10-9039-2010, 2010.

Voigt, C., U. Schumann, P. Jessberger, T. Jurkat, A. Petzold, J.-F. Gayet, M. Krämer, T. Thornberry, and D. W. Fahey Extinction and optical depth of contrails, Geophys. Res. Lett., 38, L11806, doi:10.1029/2011GL047189, 2011.

Voigt, C., P. Jessberger, T. Jurkat, S. Kaufmann, R. Baumann, H. Schlager, N. Bobrowski, G. Giuffrida, and G. Salerno: Evolution of CO_2, SO_2, HCl, and HNO_3 in the volcanic plumes from Etna, Geophys. Res. Lett., 41, 2196–2203, doi:10.1002/2013GL058974, 2014a.

Voigt, C., P. Jeßberger, T. Jurkat, S. Kaufmann, R. Baumann, H. Schlager, N. Bobrowski, G. Guffirda, G. Salerno: Reply to comment from Liotta and Rizzo, Bull. Volcanol., 76, 865, doi:10.1007/s00445-014-0865-z, 2014b.

Voshchinnikov, N., G. Videen, and T. Henning: Effective medium theories for irregular fluffy structures: aggregation of small particles, Appl. Opt. 46, 4065–4072, doi:10.1364/AO.46.004065, 2007.

Waquet, F., Peers, F., Goloub, P., Ducos, F., Thieuleux, F., Derimian, Y., Riedi, J., Chami, M., and Tanré, D.: Retrieval of the Eyjafjallajökull volcanic aerosol optical and microphysical properties from POLDER/PARASOL measurements, Atmos. Chem. Phys., 14, 1755-1768, doi:10.5194/acp-14-1755-2014, 2014.

Watson, I. M., and Oppenheimer, C.: Particle size distributions of Mount Etna's aerosol plume constrained by Sun photometry, J. Geophys. Res., 105(D8), 9823–9829, doi:10.1029/2000JD900042, 2000.

Watson, I. M., and Oppenheimer, C.: Photometric observations of Mt. Etna's different aerosol plumes, Atmos. Environ., 35, 3561–3572, doi:10.1016/S1352-2310(01)00075-9, 2001.

Yang, P., Bi, L., Baum, B.A., Liou, K.-N., Kattawar, G.W., Mishchenko, M.I., and Cole, B.: Spectrally Consistent Scattering, Absorption, and Polarization Properties of Atmospheric Ice Crystals at Wavelengths from 0.2 to 100 μm, J Atmos Sci 70:330–347, doi:10.1175/JAS-D-12-039.1, 2013.

Young, C. L., Sokolik, I. N., and Dufek, J.: Regional radiative impact of volcanic aerosol from the 2009 eruption of Mt. Redoubt, Atmos. Chem. Phys., 12, 3699-3715, doi:10.5194/acp-12-3699-2012, 2012.

Table 1. Mean parameter values in the indicated time-intervals (see Fig. 1). The parameters are: time interval, altitude, air temperature *T*, relative humidity with respect to water (RH_w); concentration (*Conc*) of particles ($d > 0.9$ μm) and effective diameter *Deff* measured with the FSSPs; real *n* and imaginary χ part of the refractive index, spherical/non-spherical partitioning ratio (*SNR*), asymmetry parameter *g*, extinction coefficients (*Ext*), and residual (*Res*) estimated from the retrievals data. (See notations in Fig. 2.)

	UT (h :min :s)	Alt. (m)	*T* (°C)	RH_w (%)	*Conc* (cm^{-3})	*Deff* (μm)	*n*	χ	*SNR* (%)	*g*	*Ext* (km^{-1})	*Res.* (%)
SV	7 :10 :28 7 :10 :45	970	17.2	36	32	2.8	1.35	0	100	0.65	0.056	6.5
BNa	7 :29 :10 7 :31 :33	3518	1.2	10	51	1.9	1.36	0	100	0.69	0.059	7.8
BNb	8 :22 :45 8 :25 :37	3202	3.4	10	25	1.5	1.37	0	100	0.70	0.020	9.4
NECa1	7 :47 :03 7 :49 :05	3656	0.3	11	40	2.2	1.36	0	100	0.66	0.059	6.7
NECa2	7 :51 :10 7 :52 :30	3645					1.38	0	100	0.65	0.120	7.4
NECb	8 :30 :13 8 :35 :30	3655	0.4	10	32	2.3	1.38	0	100	0.66	0.075	5.7

Figure captions:

Figure 1. (a) Degassing Etna plumes from North East (NEC) and Bocca Nuova (BN) craters as seen from the DLR-Falcon Research aircraft (Photo: Bernadett Weinzierl); (b) Falcon flight track over Sicily on 30 September 2011.

Figure 2. Aircraft observations of Stromboli and Etna plumes on 30 September 2011. Time series of altitude, air temperature (*T*), relative humidity with respect to water (RH_w), extinction coefficient (*Ext*) and asymmetry parameter (*g*) are shown by black points. All these parameters are referred to the left-hand y-axes. Time series of HCl, SO_2, and HNO_3 mixing ratios are shown by blue points and referred to the right-hand y-axes. Shaded areas labelled SV, BN and NEC stand for plume samplings related to Stromboli, Bocca Nuova and North East Etna craters, respectively.

Figure 3. (a) Results of the principal component analysis. First three eigenvectors (ξ_l stand for $\vec{\xi_l}$) of the angular scattering intensities (ASI) of the correlation matrix versus measured scattering angles. Values of the first three normalized eigenvalues λ_l of the eigenvectors and the remaining variability also displayed. (b) Expansion coefficient diagram: third coefficient versus second coefficient. Black points for cirrus clouds, blue points for contrails, olive points for the North-East-crater plume, violet points for the Stromboly, orange points for BNa and red points for BNb crater plumes. (c) Same as (b) but with the focus of attention on the degassing plumes. Green points for NECa and olive points for NECb crater plumes.

Figure 4. Measured (solid lines) and retrieved (solid black circles) aerosol size distributions (left panels). Measured (solid red circles) and reconstructed (solid black circles) angular scattering intensities (right panels). Stromboly (top), Bocca Nuova (middle) and North East (bottom) Etna craters plums, respectively. (See notations in Fig. 2.)

Figure 5. Probability distribution functions of the asymmetry parameter. Bocca Nuova (BNa, red) and North East (NECb, green) Etna craters plums, respectively. (See notations in Fig. 2.)

Figure 6. Refractive-index dependence of phase functions. The range of the Polar-Nephelometer operating angles is indicated by the gray bar.

NEC
BN

(a)

(b)

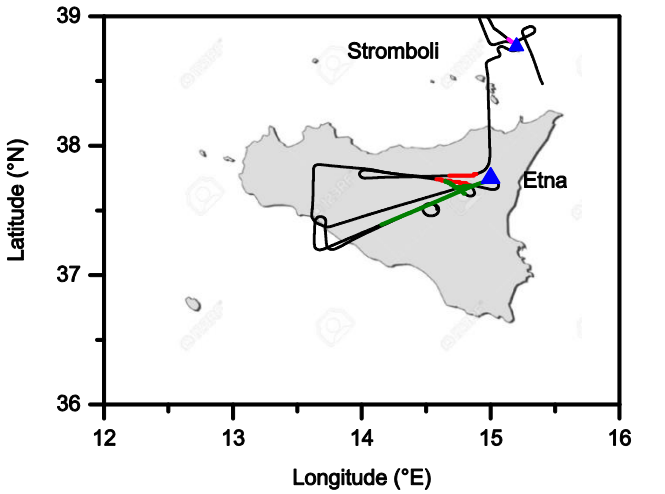
Stromboli
Etna
Latitude (°N)
Longitude (°E)
39
38
37
36
12
13
14
15
16

Fig. 1

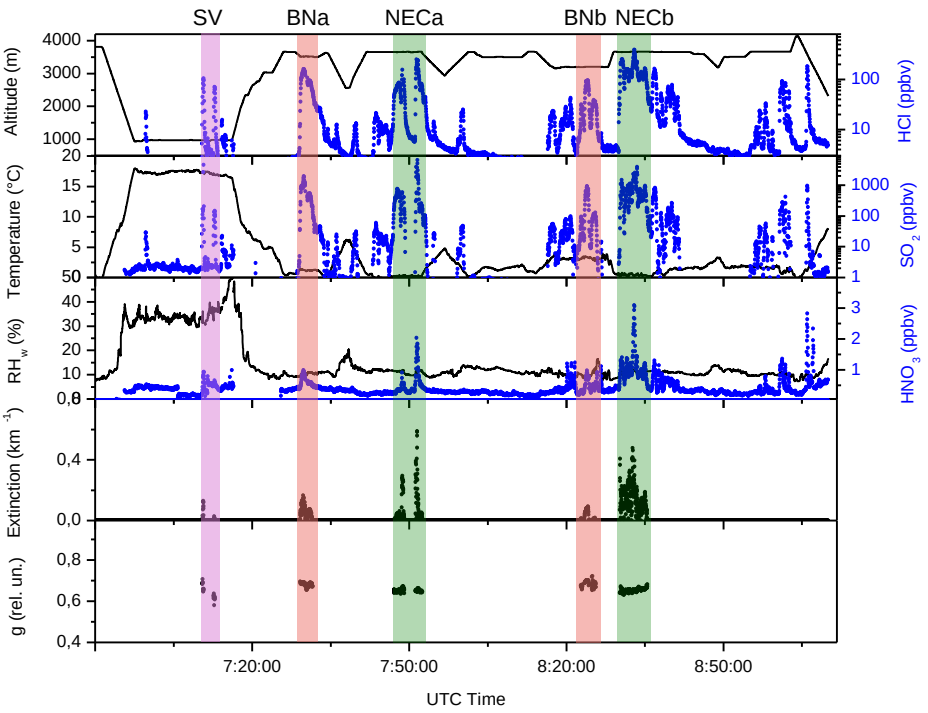
SV
BNa
NECa
BNb
NECb
Altitude (m)
4000
3000
2000
1000
HCl (ppbv)
100
10
Temperature (°C)
20
15
10
5
0
SO2 (ppbv)
1000
100
10
1
RHw (%)
40
30
20
10
0
HNO3 (ppbv)
3
2
1
Extinction (km-1)
0,8
0,4
0,0
g (rel. un.)
0,8
0,6
0,4
7:20:00
7:50:00
8:20:00
8:50:00
UTC Time

Fig. 2

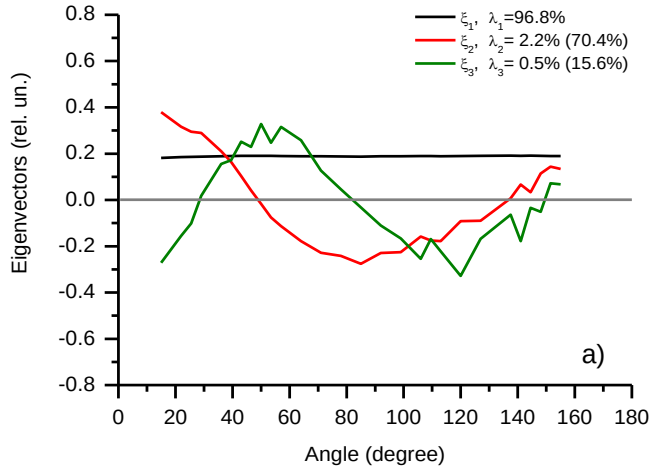
ξ1, λ1=96.8%
ξ2, λ2= 2.2% (70.4%)
ξ3, λ3= 0.5% (15.6%)
Eigenvectors (rel. un.)
Angle (degree)
a)

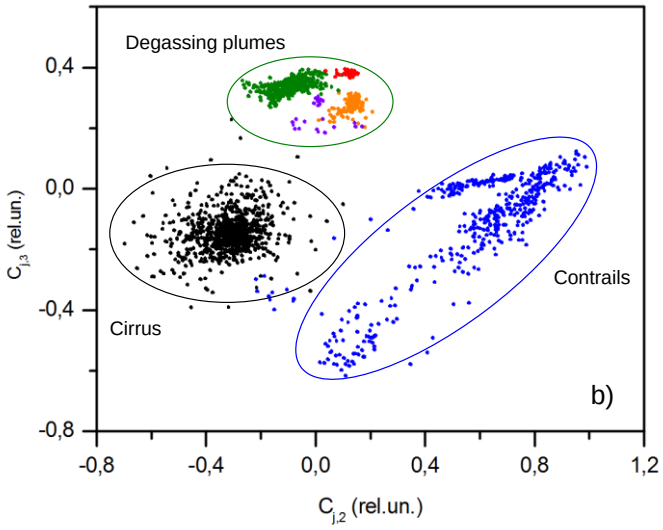
Degassing plumes
Contrails
Cirrus
b)
Cj,3 (rel.un.)
Cj,2 (rel.un.)

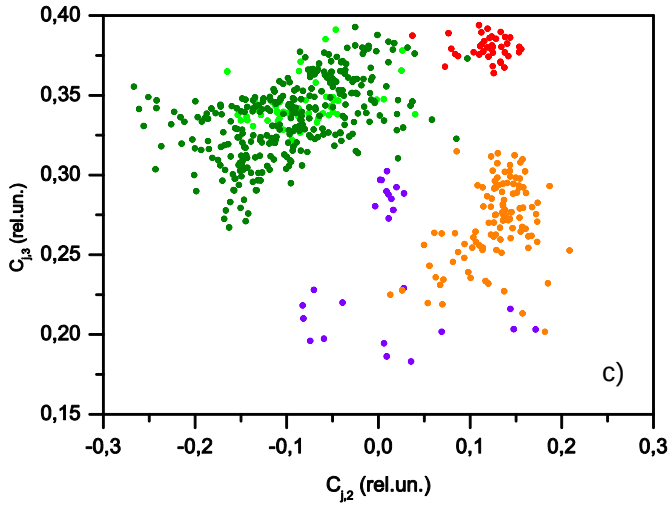
c)
Cj,3 (rel.un.)
Cj,2 (rel.un.)

Fig. 3

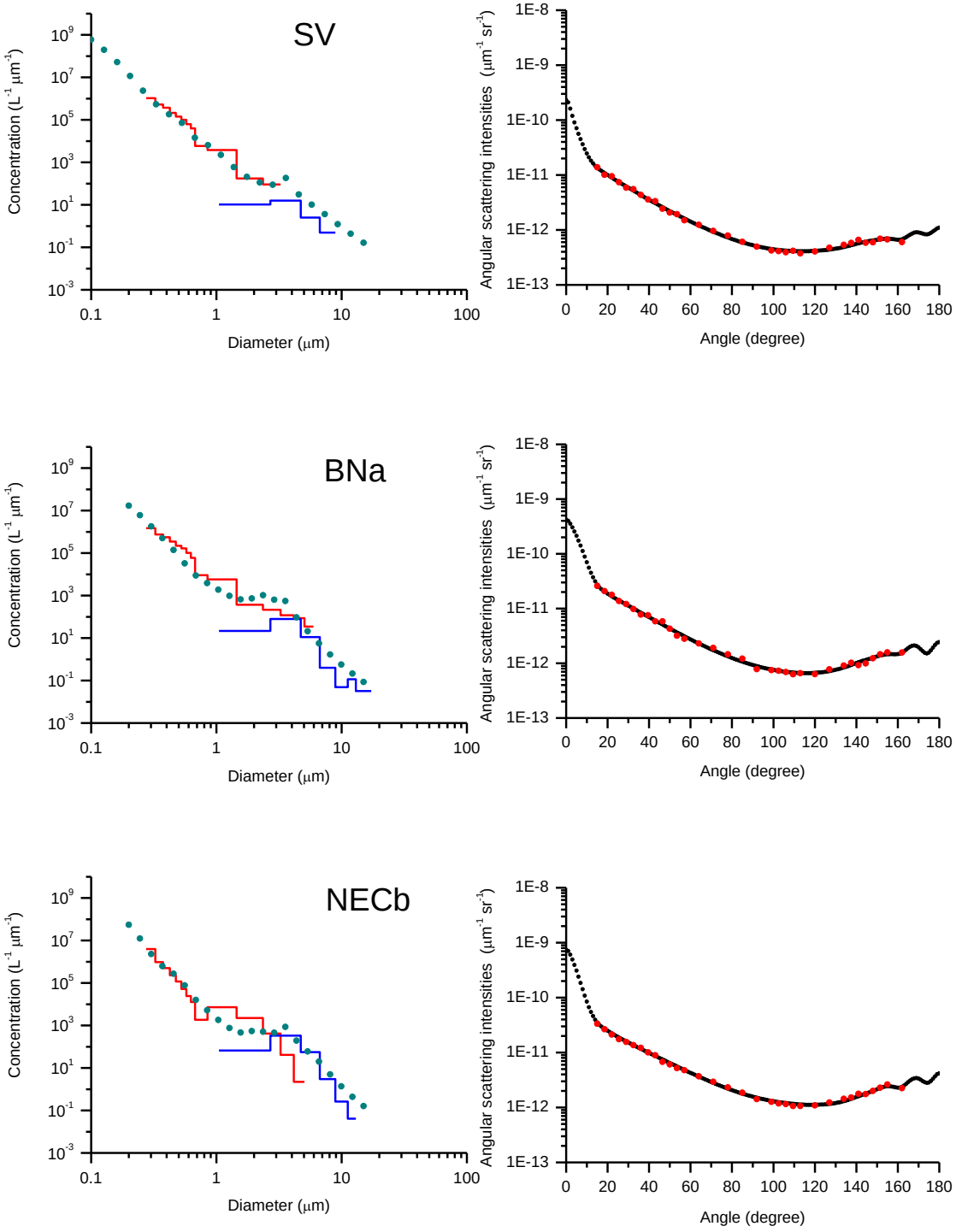
SV
BNa
NECb
Concentration (L^{-1} µm^{-1})
Diameter (µm)
Angular scattering intensities (µm^{-1} sr^{-1})
Angle (degree)

Fig. 4

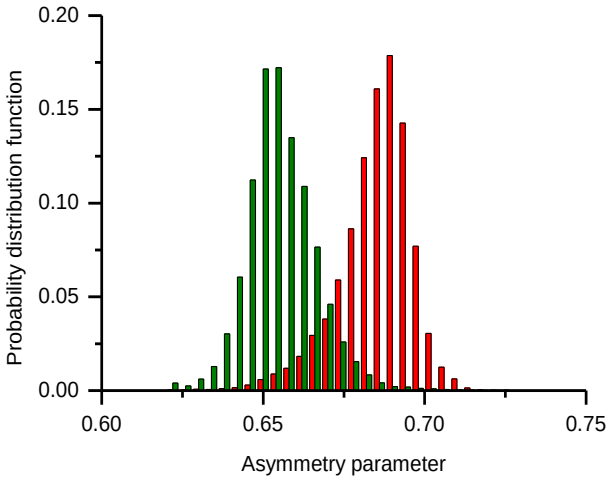
0.20
0.15
0.10
0.05
0.00
Probability distribution function
0.60
0.65
0.70
0.75
Asymmetry parameter

Fig. 5

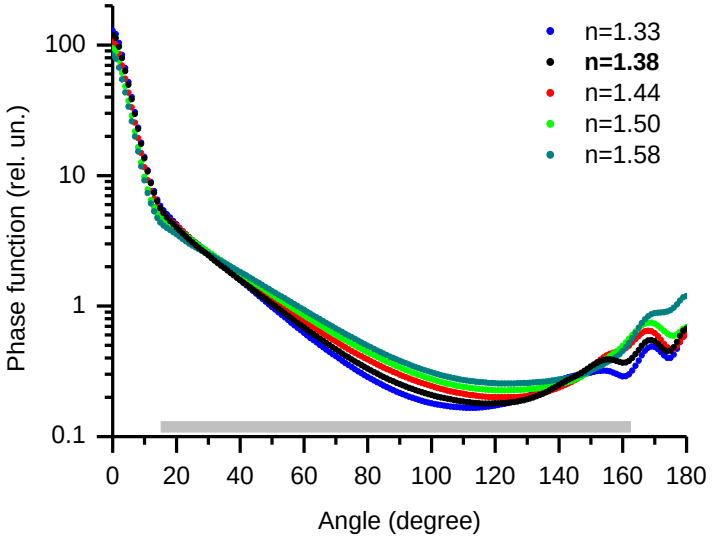
n=1.33
n=1.38
n=1.44
n=1.50
n=1.58
100
10
1
0.1
Phase function (rel. un.)
0
20
40
60
80
100
120
140
160
180
Angle (degree)

Fig. 6